100% Efficient Three-Dimensional Coronary MR Angiography with Two-Dimensional Beat-to-Beat Translational and Bin-to-Bin Affine Motion Correction

Andrew P. Aitken,[1]* Markus Henningsson,[1] Rene M. Botnar,[1] Tobias Schaeffter,[1] and Claudia Prieto[1,2]

Purpose: To develop a flexible image navigator for 3D coronary MR angiography that allows respiratory motion of variable complexity to be compensated for on different temporal scales.

Methods: A two-dimensional (2D) golden radial image navigator is proposed; translational motion is compensated for on a beat-to-beat basis, and residual affine motion is compensated for on a bin-to-bin basis in a two-step procedure. The method does not use a respiratory gating window and therefore achieves 100% scan efficiency and a predictable scan time. The proposed method was tested in 11 healthy volunteers and compared against a navigator-gated and tracked acquisition.

Results: The proposed method achieved comparable quantitative and qualitative image quality to a 6-mm navigator-gated and tracked scan while reducing the scan time by a factor of approximately 2. Combined motion correction using image navigators improved visualization of the coronary arteries in four of 11 subjects in comparison with translational correction only, and image quality was maintained in the remaining cases. In one case, visualization of the left anterior descending coronary artery was degraded using combined correction compared with translation correction only.

Conclusions: The feasibility of correcting for 2D translational motion on a beat-to-beat basis as well as affine motion on a bin-to-bin basis has been demonstrated. **Magn Reson Med 74:756–764, 2015. © 2014 The Authors. Magnetic Resonance in Medicine Published by Wiley Periodicals, Inc. on behalf of International Society of Medicine in Resonance.**

Key words: coronary MRI; image navigator; respiratory motion correction

INTRODUCTION

Free breathing three-dimensional (3D) coronary MR angiography (CMRA) is a promising noninvasive tool for the diagnosis of coronary artery disease. Despite recent advances, respiratory motion still poses a major challenge in CMRA in some subjects (1). Several approaches have been proposed to compensate for respiratory motion. Most commonly, a right hemidiaphragmatic one-dimensional "pencil beam" navigator (1DNav) is used to limit the acquisition to a small window of the respiratory cycle during end-expiration and to prospectively correct for translational motion of the heart in the superior–inferior (SI) direction (2). This has several limitations. First, only translational motion in the SI direction is corrected for; translations in the anterior–posterior (AP) and left–right directions (LR) are not accounted for, nor are rotations or nonrigid deformations, which have been found to lead to substantial motion of the coronary arteries in some subjects (3,4). However, the use of a small gating window minimizes the effects of these additional motion components at the cost of prolonged scan times, as only a fraction of the acquired data are accepted for image reconstruction (typically 20%–60%), while the remainder must be reacquired. A further limitation of the 1DNav is that the motion of the heart is not measured directly by the navigator but is inferred from the motion of the right hemidiaphragm using a scaling factor (typically 0.6) (5). Residual motion artifacts may therefore be apparent in the reconstructed images.

To overcome these limitations, two-dimensional (2D) and 3D image navigators (iNav) have been proposed recently (6–17). In these approaches, the motion of the heart is measured directly, allowing translational motion correction to be performed in two or three directions, with some methods also allowing for affine motion correction (6,9,12–15). Tracking the motion of the heart directly allows a much larger gating window to be used, increasing the scan efficiency to or close to 100%.

[1]King's College London, Division of Imaging Sciences, and Biomedical Engineering, St. Thomas' Hospital, London, UK.

[2]Pontificia Universidad Católica de Chile, Escuela de Ingeniería, Santiago, Chile.

Grant sponsor: Medical Research Council (MRC); Grant number: MR/L009676/1; Grant sponsor: The Centre of Excellence in Medical Engineering (funded by the Wellcome Trust and EPSRC); Grant number: WT 088641/Z/09/Z; Grant sponsor: Department of Health via the National Institute for Health Research (NIHR) comprehensive Biomedical Research Centre award to Guy's & St Thomas' National Health Service (NHS) Foundation Trust, in partnership with King's College London and King's College Hospital NHS Foundation Trust; Grant sponsor: Andrew P. Aitken's Ph.D. studentship is funded by Philips Healthcare.

*Correspondence to: Andrew Aitken, M.Sc., Division of Imaging Sciences and Biomedical Engineering, The Rayne Institute, 4th Floor, Lambeth Wing, St. Thomas' Hospital, London, SE1 7EH, United Kingdom. E-mail: andrew.aitken@kcl.ac.uk

The views expressed are those of the authors and not necessarily those of the NHS, the NIHR, or the Department of Health.

Received 4 June 2014; revised 31 July 2014; accepted 21 August 2014

DOI 10.1002/mrm.25460
Published online 18 September 2014 in Wiley Online Library (wileyonlinelibrary.com).

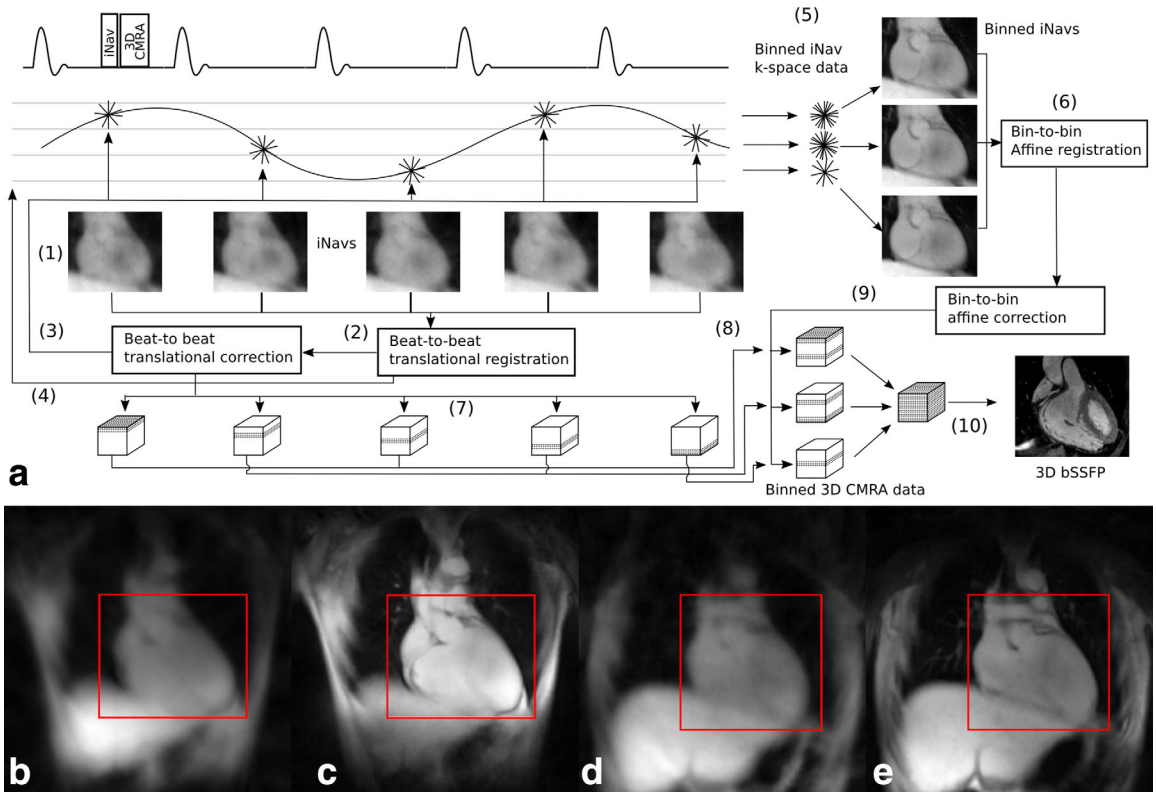

FIG. 1. **a:** Motion estimation and correction scheme. Motion estimation: (1) A 2D GR iNav is acquired prior to each shot of a 3D Cartesian CMRA sequence and reconstructed following low pass-filtering. (2) Beat-to-beat translational motion in the SI and LR directions is estimated from the iNavs using template matching. (3) The translational motion estimation is used to correct the iNav k-space data on a beat-to-beat basis. (4) The estimated translational motion in the SI direction is used to bin the iNav data. (5) The binned iNav data are reconstructed to produce high spatial resolution iNavs for each of 10 respiratory states (bins). (6) Affine registration is performed to estimate residual affine motion between bins. Motion correction: (7) Beat-to-beat 2D translational motion correction is performed in k-space for each shot of the 3D Cartesian CMRA scan. (8) The 3D CMRA data are binned according to the estimated SI translational motion. (9) Correction for residual affine motion is performed in k-space for each set of binned 3D CMRA data. (10) The binned data are combined and reconstructed to produce the motion corrected 3D CMRA image. **b-e:** Examples of acquired navigators for two volunteers and ROIs used for registration. Panels b and d show beat-to-beat navigators; panels c and e show binned navigators.

Methods in which iNavs are used can be divided into two groups of approaches. In the first group, a low spatial resolution or undersampled iNav is acquired during each cardiac cycle, providing an image of sufficient quality to allow translational motion to be estimated via image registration for each heartbeat ("beat-to-beat" estimation) (7,8,10,11,16,17); however, the relatively low image quality of these beat-to-beat methods makes robust estimation of nonrigid motion difficult. In the second group, iNavs for several respiratory states (so-called "bins") are acquired over several cardiac cycles (6,9,12–15). These "bin-to-bin" methods provide iNavs with a reduced temporal resolution with respect to beat-to-beat methods, but yield iNavs with a higher spatial resolution and higher signal-to-noise ratio (SNR), allowing nonrigid motion to be estimated between the respiratory bins. However, due to the decreased temporal resolution, intra-bin motion may leave residual motion artifacts.

In this study, we propose a new image navigator approach that allows both beat-to-beat translational motion and bin-to-bin affine motion to be estimated using the same iNav data. This is achieved by acquiring the iNav with a golden radial (GR) k-space trajectory (18). The GR trajectory provides a relatively uniform distribution of samples in the angular direction of k-space for an arbitrary imaging time, thus allowing the retrospective reconstruction of images at different temporal resolution, spatial resolution, and SNR. The 2D GR iNav is interleaved with a 3D Cartesian CMRA scan with no gating window (100% scan efficiency) and the motion estimation derived from the iNav is used to correct the 3D CMRA scan in k-space using a two-step procedure. First, translational motion is corrected for on a beat-to-beat basis. Second, the 3D CMRA is binned according to the translational motion in the SI direction and residual nonrigid motion is corrected for on a bin-to-bin basis using an affine motion model. Moreover, the proposed method offers the flexibility to choose between translation only or translation and affine correction retrospectively according to the complexity of the motion of each subject. The proposed approach was tested in vivo in healthy subjects and compared with a conventional gated 1DNav scan. Results using the proposed approach for beat-to-beat translation correction only and combined translation and affine correction were also compared.

METHODS

A highly undersampled 2D GR coronal iNav was acquired for each cardiac cycle, in place of the 1DNav. A coronal orientation was chosen to minimize aliasing artifacts originating from hyperintense subcutaneous fat. The iNav was interleaved with the 3D CMRA sequence using an instantaneous interleaved scanning framework (19). The general motion correction and estimation procedure is illustrated in Figure 1.

Beat-to-Beat Motion Estimation and Correction

Each highly undersampled iNav was reconstructed using gridding reconstruction (20) using an iterative estimate of the sample density weights (21), which also provides a low pass filtering effect for the case of undersampled radial data. This resulted in a series of low spatial resolution 2D images with high temporal (beat-to-beat) resolution. Translational motion in two dimensions (SI and LR) was estimated using a template-matching algorithm over a region of interest (ROI) placed on the heart, with normalized cross-correlation as the similarity measure and with the first image used as a reference. The region of interest was placed manually for each subject, with examples shown in Figure 1b–e. The mean sizes of the ROIs in the SI and LR directions were 136 ± 18 mm and 154 ± 14 mm, respectively. The iNav k-space data and the 3D CMRA data were then corrected for 2D translational motion by multiplying the data for each heartbeat by an appropriate linear phase (22).

Bin-to-Bin Motion Estimation and Correction

Based on the estimated beat-to-beat motion in the SI direction, the translational corrected iNav data were binned into 10 equally populated respiratory states. The combined k-space data for each bin were reconstructed to provide a high spatial resolution iNav for each bin. Because these "binned" iNavs were already corrected for translational motion prior to reconstruction, they depicted only the residual nonrigid motion of the heart. This residual motion was then estimated using 2D affine image registration with an ROI placed around the heart. Normalized cross-correlation was used as the similarity measure, and the end-exhale bin was used as the reference state. The affine registration yielded a 2D affine motion matrix for each bin, which maps points in the image corresponding to a particular bin back to the reference state and takes the form

$$A = \begin{bmatrix} A_{11} & A_{12} & T_x \\ A_{21} & A_{22} & T_y \\ 0 & 0 & 1 \end{bmatrix},$$

where the elements A_{ij} represent scaling, shearing, and rotation in the coronal plane, and T_x and T_y represent translations in the SI and LR directions, respectively. The translational-corrected 3D CMRA data were binned in the same way as for the iNav data. They were then corrected for residual affine motion by applying an additional linear phase to the data according to T_x and T_y and then modifying the k-space trajectories for each bin as follows (22):

$$k_c = Bk,$$

where k and k_c are matrices of size $2 \times N$, which contain the k-space coordinates of the N points on the nominal and corrected trajectories, respectively, and

$$B = \begin{bmatrix} A_{11} & A_{21} \\ A_{12} & A_{22} \end{bmatrix}^{-1}.$$

In Vivo Experiments

Eleven healthy adult subjects were scanned on a 1.5T Philips Achieva scanner (Philips Healthcare, Best, Netherlands). All subjects provided written informed consent before undergoing MRI, and the study was approved by the Institutional Review Board. 3D CMRA was performed using a Cartesian balanced steady-state free precession sequence using the following parameters: isotropic voxel size = 1.4 mm; field of view = $300 \times 300 \times 120$ mm^3; echo time (TE)/repetition time (TR) = 2.1/4.1 ms; flip angle = 70°; T_2 preparation (TE = 30 ms); fat saturation prepulse; subject-specific acquisition window (98–131 ms); and trigger delay targeting the middiastolic rest period. For the 2D GR iNav, a spoiled gradient echo sequence was performed using the following parameters: pixel size = 1.5×1.5 mm^2; slice thickness = 20 mm; field of view = 300×300 mm^2; 28 angular profiles per cardiac cycle; acquisition window = 89 ms; TE/TR = 1.6/3.2 ms; flip angle = 5°. This resulted in a sevenfold reduction in the number of readouts for each beat-to-beat iNav compared with a fully sampled Cartesian scan.

CMRA was performed twice for each subject within the same session; once with a hemidiaphragmatic 1DNav with a 6 mm gating window and prospective correction for SI motion and a once with the proposed iNav and no gating window. The order of the two scans was randomized.

Image reconstruction was performed offline in MATLAB (Mathworks, Natick, Massachusetts, USA). Four sets of CMRA images were reconstructed: 1) hemidiaphragmatic 1DNav scan, 2) iNav scan with no motion correction, 3) iNav scan with beat-to-beat translational correction only, and 4) iNav scan with beat-to-beat translational correction and bin-to-bin affine correction. For cases 1–3, reconstruction was performed using a uniform fast Fourier transform. For case 4, the affine motion correction modified the k-space trajectories so that they no longer fell on a Cartesian grid. This introduced the requirement for a regridding operation prior to the Fourier transform.

The reconstructed volumes were reformatted using a curved reformat to visualize the left anterior descending coronary artery (LAD) and the right coronary artery (RCA) using dedicated software (23). Visualized RCA and LAD vessel lengths and sharpness were measured. Vessel sharpness was calculated as the ratio of the maximum intensity to the maximum gradient across the vessel profile, such that 100% sharpness represented a

Table 1
Gating Efficiencies and Motion Parameter Ranges for Each Subject

Subject no.	Gating efficiency, %	Beat-to-beat translation (max – min), mm $\begin{bmatrix} T_x \\ T_y \end{bmatrix}$	Bin-to-bin rotation, scaling and shear (max – min) $\begin{bmatrix} A_{11} & A_{12} \\ A_{21} & A_{22} \end{bmatrix}$		Bin-to-bin translation (max – min), mm $\begin{bmatrix} T_x \\ T_y \end{bmatrix}$
1	29	15.938 2.679	0.067 0.008	0.006 0.008	1.956 0.432
2	55	13.125 1.339	0.066 0.008	0.004 0.010	2.251 0.525
3	45	9.643 2.813	0.017 0.017	0.006 0.004	2.102 1.234
4	43	32.009 4.420	0.075 0.021	0.021 0.013	0.548 0.452
5	55	25.045 2.813	0.098 0.017	0.026 0.019	0.876 0.422
6	51	18.482 3.616	0.079 0.011	0.005 0.012	0.480 0.395
7	49	15.402 2.946	0.064 0.014	0.033 0.015	0.917 0.854
8	47	14.598 3.348	0.108 0.008	0.031 0.016	1.605 0.695
9	43	10.982 3.080	0.063 0.009	0.043 0.004	0.445 0.362
10	60	17.946 2.143	0.052 0.010	0.015 0.004	1.002 0.300
11	49	8.705 2.277	0.037 0.012	0.008 0.005	1.158 0.339

maximum signal intensity change at the vessel edge. Qualitative image scoring was performed by two independent, experienced observers (M.H. and R.M.B., who have 5 and 20 years of experience in cardiac MRI, respectively) who were blinded to the technique employed. The scores from the two observers were averaged prior to further analysis.

The vessel sharpness and length measurements were tested for normality using the Shapiro-Wilk test and for sphericity (equality of variance between all reconstruction methods) using the Mauchly test. The difference between these measures for the four reconstruction approaches were analyzed using repeated measures analysis of variance (rANOVA). The Greenhouse-Geisser correction was used to adjust the degrees of freedom and associated p-values for all rANOVA tests [as the assumption of equal variance was violated for LAD vessel sharpness: χ^2 (5) = 18.177, $P = 0.011$; LAD length: χ^2 (5) = 27.905, $P < 0.001$]. Differences in visual scores for the four reconstruction approaches were assessed using the Friedman test. Pairwise differences between individual reconstruction approaches for all measures were compared using Wilcoxon signed rank tests (as the assumption of normality of pairwise differences was violated for RCA vessel length between the translation only case and the translation plus affine case ($P = 0.043$)) with a Bonferroni post hoc correction for multiple comparisons.

RESULTS

Scans were completed and successfully reconstructed with the proposed method in all subjects. The range of measured motion parameters with the proposed approach for beat-to-beat translation and bin-to-bin affine motion is shown for each volunteer in Table 1. Large beat-to-beat translational motion along the SI direction was detected and corrected in the beat-to-beat step, along with smaller translations in the LR direction. Subsequently, only small residual translation parameters were observed in the bin-to-bin step. Examples of the reconstructed beat-to-beat (low spatial resolution) and bin-to-bin (high spatial resolution) image navigators are shown in Figure 1b–e.

The 1DNav scan efficiency was 47.8 ± 7.8 across all subjects. The 1DNav scan efficiency for each subject is

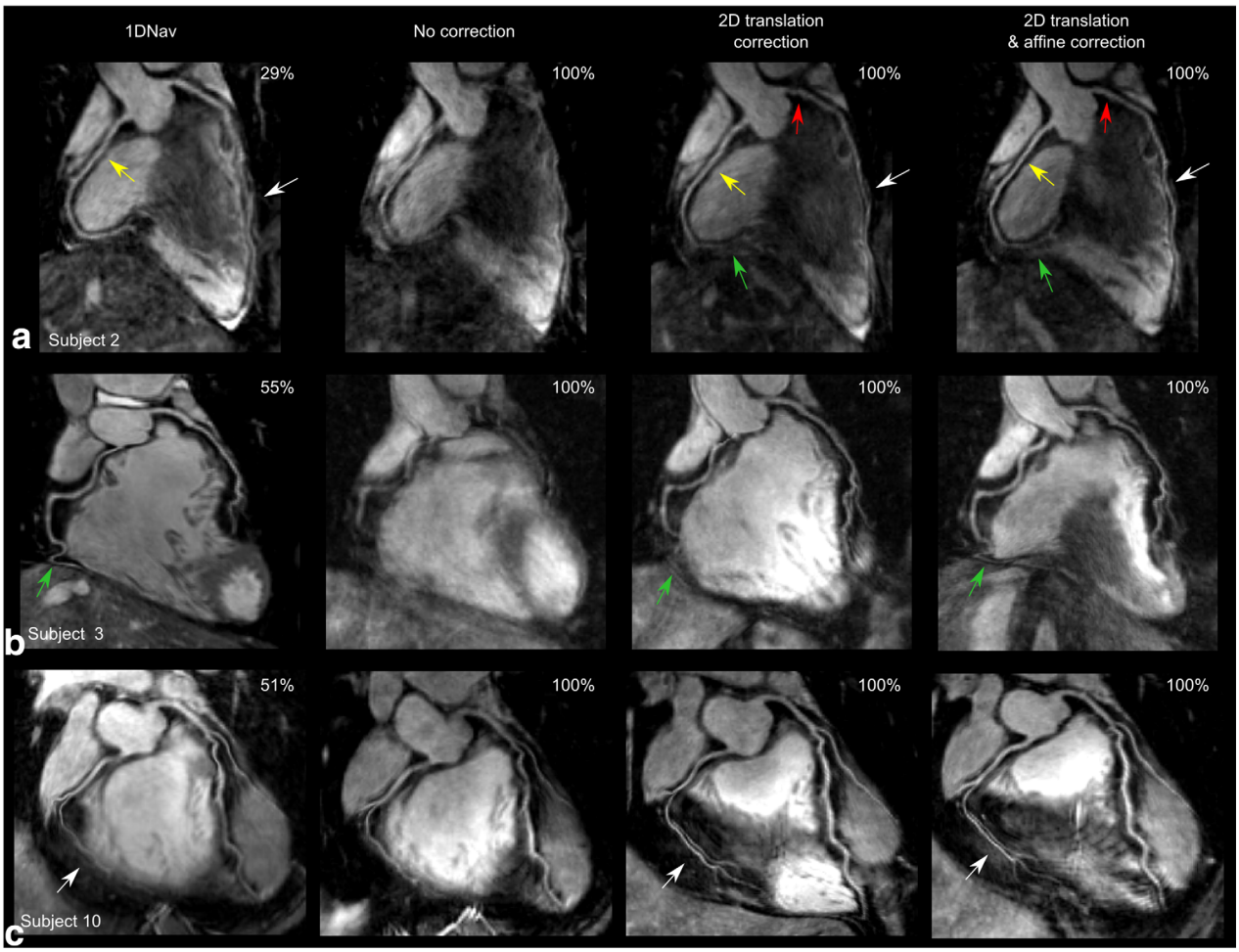

FIG. 2. Sample reformatted images showing the LAD and RCA for three subjects (one subject per row). The columns show, from left to right: 1D navigator with 6-mm respiratory gating window, uncorrected scan (no gating window), iNav with translation correction only (no gating window), and iNav with translation and affine correction (no gating window).

shown in Table 1. The subject-specific acceleration factor relating the scan time of the proposed iNav compared with that of the 1DNav ranged between 1.7 and 3.4, with a mean acceleration factor of 2.0 across all subjects.

Sample reformatted images showing the RCA and LAD for three subjects are shown in Figure 2. For subject 2 (Fig. 2a), the RCA was well visualized in the 1DNav scan but was blurred and obscured by artifact when no gating or correction was used. Visualization of the RCA was improved relative to the uncorrected case when 2D beat-to-beat translation only was applied, but the distal segment was still obscured (green arrows). Additional correction for bin-to-bin affine motion improved the visualization of the distal segment (green arrows) and led to improved sharpness of the proximal segment relative to the 1DNav case (yellow arrows). For this subject, the LAD was blurred in the 1DNav and uncorrected cases but appeared much sharper when beat-to-beat translation correction was applied (white arrows), despite the decrease in scan time by a factor greater than 3. Additional bin-to-bin affine correction further improved the sharpness of the proximal segment of the LAD (red arrows).

For subject 3 (Fig. 2b), both the LAD and RCA were well depicted using the 1DNav scan but were obscured by artifact in the uncorrected case. Beat-to-beat translational correction improved visualization (green arrows), but the distal segment of the RCA remained obscured. Additional bin-to-bin affine correction increased the visible vessel length of the RCA. For subject 10 (Fig. 2c), the sharpness and visible length of both the LAD and RCA improved for the case of 2D beat-to-beat translational correction compared with the 1DNav case (white arrows), but there was little appreciable difference between the translation only case and the translation and affine case.

Quantitative vessel sharpness and visible vessel length measurements are shown in Figure 3, along with the qualitative visual scores. There were significant differences in vessel sharpness between reconstruction approaches for the both the LAD [$F(1.668,11) = 10.79$, $P = 0.006$] and RCA [$F(2.201,11) = 14.259$, $P < 0.001$]. There were also significant differences in the visible vessel length between reconstruction approaches for both the LAD [$F(1.180,11) = 9.064$, $P = 0.036$] and RCA [$F(2.112,11) = 8.095$, $P = 0.009$]. Wilcoxon signed rank

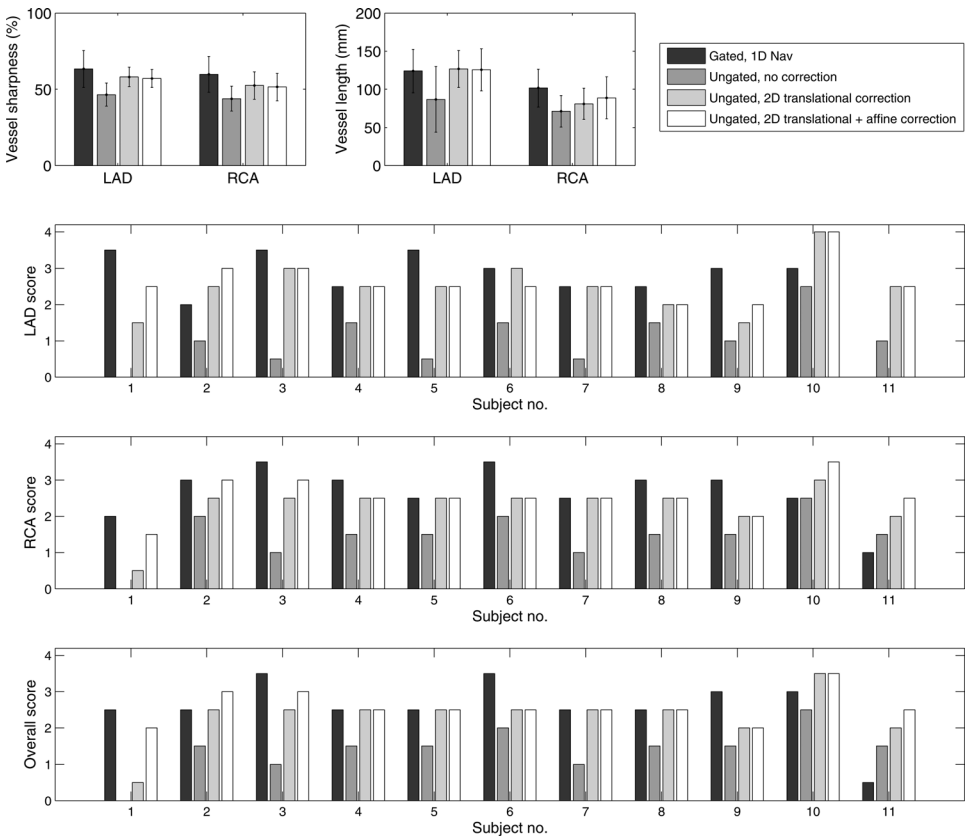

FIG. 3. Mean (±1 standard deviation) of vessel sharpness and visible vessel lengths across all subjects and qualitative visual scores for each subject.

tests revealed there were no significant differences in vessel sharpness or length between any pair of reconstruction approaches.

There were significant differences in all three visual scores between the four correction methods [LAD: χ^2 $(11) = 20.41$, $P < 0.001$; RCA: χ^2 $(11) = 20.84$, $P < 0.001$; overall: χ^2 $(11) = 20.10$, $P < 0.001$]. Post hoc analysis revealed that for each score, there was a significant difference between the uncorrected case and the translation only case and between the uncorrected case and the translation plus affine case ($P = 0.041$ for all cases).

Because no significant differences were found between the 1DNav case and the proposed method, or between the translation only and the translation plus affine cases, images for three additional subjects are shown in Figure 4 to further demonstrate the value and limitations of the proposed method. Figure 4a shows the results for subject 11, which was the best case for the proposed method in terms of overall visual score when compared with the 1DNav case. There was a substantial improvement in the visualization of the coronary arteries using the iNav compared with the 1DNav case, despite the reduction in scan time of approximately 2 in the former case. Figure 4b and 4c (subjects 9 and 6, respectively) shows the worst cases for the proposed method compared with the 1DNav case, where it can be seen that the image quality is somewhat degraded using the proposed approach.

In one subject (subject 6), the LAD score was lower for the translation plus affine case compared with the translation only case. This case is shown in Figure 4c, where it can be seen that the proximal segment of the LAD is slightly blurred in the affine plus translation case compared with the translation only and the 1DNav case. In all other subjects, the LAD score for the affine case was greater than ($n = 3$ cases) or equal to the translation only case. For all subjects, the RCA score and overall score for the translation plus affine case was greater than ($n = 5$ cases for RCA score, $n = 4$ for overall score) or equal to the translation only case.

DISCUSSION

A novel approach to motion correction for 3D CMRA has been proposed in which the same image navigator data are used to correct first for 2D translational beat-to-beat motion and second for residual 2D affine motion on a bin-to-bin basis. This offers an advantage over other proposed methods, which provide only 2D translational motion correction on a beat-to-beat basis, or affine correction on a bin-to-bin basis. Using the framework described by Henningsson et al. (19), it is straightforward to switch between a 2D golden radial acquisition for the iNav and a 3D Cartesian acquisition for the CMRA scan. This allows the properties of the golden radial acquisition to be exploited such that motion information can be extracted at different temporal resolutions while maintaining the SNR benefit of a Cartesian scheme for the CMRA scan. Nevertheless, the proposed navigator could

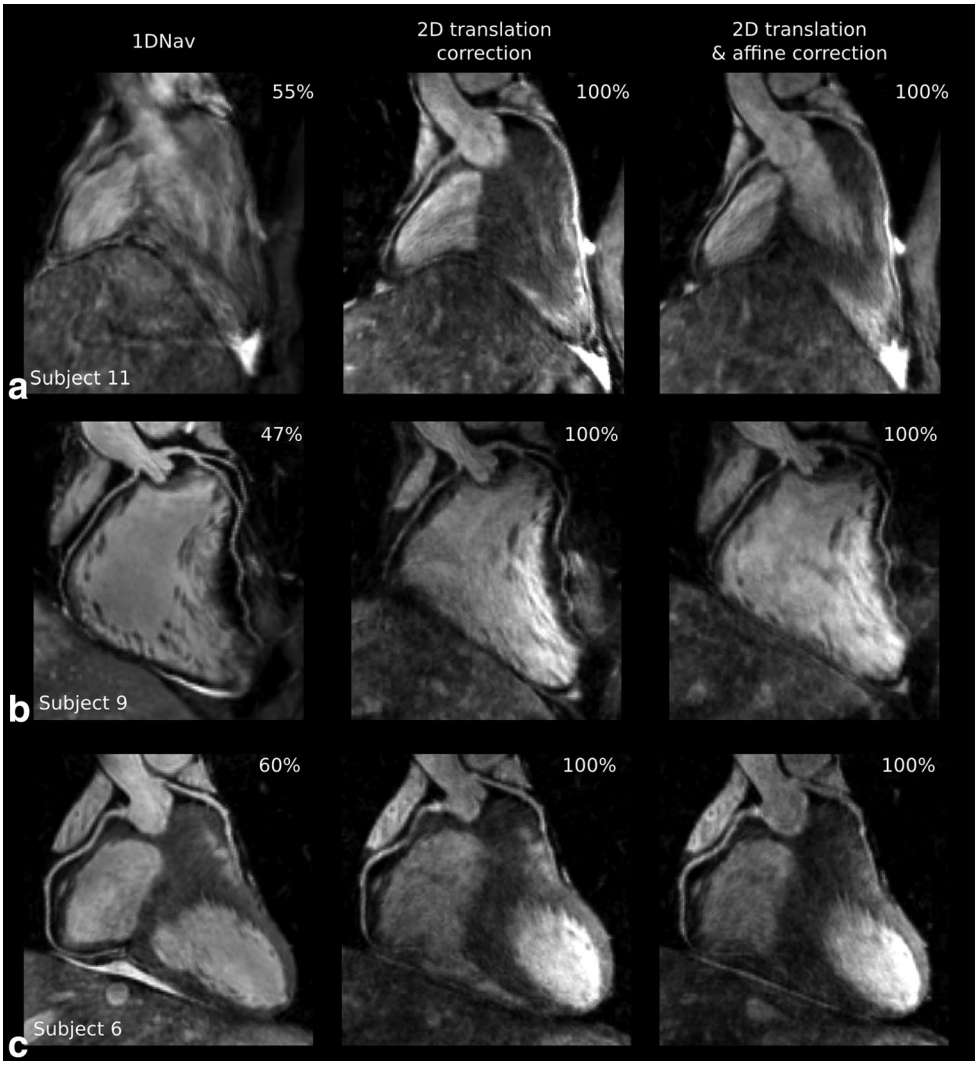

FIG. 4. Images and vessel scores for three subjects. **a:** Subject in whom the iNav provided the greatest increase in image quality compared with the 1DNav case. **b, c:** Cases in which the iNav provided the greatest decrease in image quality compared with the 1DNav case. Panel c also shows the only case in which the image score was lower for the LAD after additional affine correction compared with the translation only case.

easily be combined with any CMRA acquisition using the current framework.

There were no significant differences in any of the image quality measures between the 1DNav case and the proposed method, despite a reduction in scan time by a factor of approximately 2 using the proposed approach. In some cases, the proposed method outperformed the 1DNav, despite the reduction in scan time. This is likely because the iNav tracks the heart directly rather than inferring the motion from the diaphragm, which also avoids problems due to subject specific tracking factors (5) and to hysteresis effects between the motion of the diaphragm and that of the heart (24). Furthermore, the iNav tracks motion in two dimensions rather than one.

However, in four cases there was a reduction in the overall image score using the proposed method compared with the 1DNav scan. This could be due to a number of factors, including through-plane motion and nonrigid motion components that are not accurately modeled or measured using an affine image registration model. The effects of residual motion artifacts could be reduced by removing extreme respiratory positions, and reconstruction could be performed using parallel imaging and/or compressed sensing (25–28) to compensate for the resultant undersampling. Furthermore, the CMRA scan was fully sampled in this study, thus the scan time could potentially be reduced further using parallel imaging and/or compressed sensing reconstruction. This is being investigated in current work.

Another potential source of residual artifacts is through-plane motion and differing motion for different positions in the AP direction, which cannot be captured by the 2D navigator. The proposed approach could potentially be extended to include a trailing sagittal iNav acquired after the 3D CMRA data, as well as the leading coronal iNav, as was used in this study. 3D motion parameters could then be extracted in a manner similar to that described by Wu et al. (17). Alternatively, a 3D GR iNav could be employed using trajectories similar to those proposed by Piccini et al. (29) and Chan et al. (30), with parallel imaging and/or compressed sensing used to recover iNavs from highly undersampled 3D data.

Compared with the beat-to-beat translation only case, there were no significant differences when additional bin-to-bin affine correction was applied, although it is clear from Figure 3 that there was an improvement in several cases when the additional affine correction is performed, particularly for the RCA. This was not necessarily reflected in an increase in the measured vessel sharpness, which is likely to be because the vessel sharpness was only measured across segments of the vessel that were clearly visible in all cases, hence it does not reflect the improved visualization and sharpness of the distal RCA when the additional affine correction was performed.

In terms of visual score, the translation plus affine method performed equal to or better than the translation only method in all but one of the cases. It is possible that in this case, the measured affine motion did not accurately describe the motion across the whole heart because only the quality of the LAD was affected. However, because the proposed method allows both cases to be reconstructed from the same data, this is not a severe limitation. Related to this, one problem yet to be explored is how to interpret images reconstructed using the translation only and translation plus affine methods if the images reconstructed with one method shows a stenosis and the other does not. Further work is required to determine the accuracy of each approach in patients. However, it is likely that the addition of affine correction may make a more notable difference in patients with abnormal anatomy, who may exhibit more complex motion than healthy subjects. It would also be interesting to explore whether the cases for which additional affine correction is likely to be beneficial can be predicted from the navigator data.

The total reconstruction time for the proposed method was approximately 8 min using 12 CPUs (Intel Xeon 2.70GHz). This included approximately 5.5 min for image navigator reconstruction and motion estimation and 2.5 min for motion correction and reconstruction of the 3D CMRA dataset. The translation only case took approximately 30 s less than the translation and affine case, as no regridding operation was required for the 3D CMRA data in this case. The time taken for the proposed method was considerably longer than the time required for the 1DNav case (approximately 1 min on the same machine), but is not prohibitive for clinical use. The reconstruction was not optimized for computational speed.

Ingle et al. (31) recently proposed a similar two-step motion correction method in which 3D translational motion is corrected for on a beat-to-beat basis, followed by nonrigid correction using an autofocus method, with the translational motion estimates derived using the image navigators used to constrain the search space for the algorithm. This method differs from the proposed method in that the nonrigid motion is not directly measured using the image navigator but is instead estimated based on the optimization of an image quality metric, using the navigator information as a constraint. An advantage of the autofocus method is that it can deal with more complex nonrigid motion that cannot be accurately described using an affine model. However, the computational burden is much higher for autofocus techniques, as the gridding and Fourier transformation steps must be performed for each point in the search space (405 points in Ingle et al.), whereas in the proposed method this step is only performed once.

Another difference between the proposed method and the method described by Ingle et al. is that the proposed iNav is compatible with any sampling scheme for the 3D CMRA scan, whereas the performance of autofocus methods depends on the nature of the motion artifacts, which in turn depends on the sampling pattern. For example, Ingle et al. proposed a cones trajectory that leads to motion artifacts in the form of blurring, which can be removed using the gradient entropy focusing metric. In future work, it will be interesting to compare the two methods and to explore the estimation and correction of more complex nonrigid motion using the proposed method.

CONCLUSIONS

A novel flexible golden radial image navigator has been proposed for motion compensated coronary MRA. The proposed navigator allowed both translational motion to be estimated for each heartbeat and residual affine motion to be estimated for 10 respiratory positions. Initial results for 11 subjects were presented. In four subjects, additional affine motion considerably improved visualization of the coronary arteries—in particular, the distal segment of the RCA—when compared with correction for translation only. The proposed method offers the flexibility to choose between translation only or translation and affine correction retrospectively according to the complexity of the motion of each subject.

REFERENCES

1. Henningsson M, Botnar RM. Advanced respiratory motion compensation for coronary MR angiography. Sensors 2013;13:6882–6899.
2. Wang Y, Rossman PJ, Grimm RC, Riederer SJ, Ehman RL. Navigator-echo-based real-time respiratory gating and triggering for reduction of respiration effects in three-dimensional coronary MR angiography. Radiology 1996;198:55–60.
3. Manke D, Nehrke K, Börnert P, Rösch P, Dössel O. Respiratory motion in coronary magnetic resonance angiography: a comparison of different motion models. J Magn Reson Imaging 2002;15:661–671.
4. Shechter G, Ozturk C, Resar JR, McVeigh ER. Respiratory motion of the heart from free breathing coronary angiograms. IEEE Trans Med Imaging 2004;23:1046–1056.
5. Wang Y, Riederer SJ, Ehman RL. Respiratory motion of the heart: kinematics and the implications for the spatial resolution in coronary imaging. Magn Reson Med 1995;33:713–719.
6. Bhat H, Ge L, Nielles-Vallespin S, Zuehlsdorff S, Li D. 3D radial sampling and 3D affine transform-based respiratory motion correction technique for free-breathing whole-heart coronary MRA with 100% imaging efficiency. Magn Reson Med 2011;65:1269–1277.
7. Dewan M, Hager GD, Lorenz CH. Image-based coronary tracking and beat-to-beat motion compensation: feasibility for improving coronary MR angiography. Magn Reson Med 2008;60:604–615.
8. Henningsson M, Koken P, Stehning C, Razavi R, Prieto C, Botnar RM. Whole-heart coronary MR angiography with 2D self-navigated image reconstruction. Magn Reson Med 2012;67:437–445.
9. Henningsson M, Prieto C, Chiribiri A, Vaillant G, Razavi R, Botnar RM. Whole-heart coronary MRA with 3D affine motion correction using 3D image-based navigation. Magn Reson Med 2014;71:173–181.
10. Henningsson M, Smink J, Razavi R, Botnar RM. Prospective respiratory motion correction for coronary MR angiography using a 2D image navigator. Magn Reson Med 2013;69:486–494.
11. Kawaji K, Spincemaille P, Nguyen TD, Thimmappa N, Cooper MA, Prince MR, Wang Y. Direct coronary motion extraction from a 2D fat

image navigator for prospectively gated coronary MR angiography. Magn Reson Med 2014;71:599–607.
12. Pang J, Bhat H, Sharif B, Fan Z, Thomson LEJ, LaBounty T, Friedman JD, Min J, Berman DS, Li D. Whole-heart coronary MRA with 100% respiratory gating efficiency: self-navigated three-dimensional retrospective image-based motion correction (TRIM). Magn Reson Med 2014;71:67–74.
13. Pang J, Sharif B, Arsanjani R, Bi X, Fan Z, Yang Q, Li K, Berman DS, Li D. Accelerated whole-heart coronary MRA using motion-corrected sensitivity encoding with three-dimensional projection reconstruction. Magn Reson Med 2015;73:284–291.
14. Prieto C, Doneva M, Usman M, Henningsson M, Greil G, Schaeffter T, Botnar RM. Highly efficient respiratory motion compensated free-breathing coronary mra using golden-step Cartesian acquisition. J Magn Reson Imaging 2015;41:738–746.
15. Schmidt JFM, Buehrer M, Boesiger P, Kozerke S. Nonrigid retrospective respiratory motion correction in whole-heart coronary MRA. Magn Reson Med 2011;66:1541–1549.
16. Scott AD, Keegan J, Firmin DN. Beat-to-beat respiratory motion correction with near 100% efficiency: a quantitative assessment using high-resolution coronary artery imaging. Magn Reson Imaging 2011; 29:568–578.
17. Wu HH, Gurney PT, Hu BS, Nishimura DG, McConnell M V. Free-breathing multiphase whole-heart coronary MR angiography using image-based navigators and three-dimensional cones imaging. Magn Reson Med 2013;69:1083–1093.
18. Winkelmann S, Schaeffter T, Koehler T, Eggers H, Doessel O. An optimal radial profile order based on the Golden Ratio for time-resolved MRI. IEEE Trans Med Imaging 2007;26:68–76.
19. Henningsson M, Mens G, Koken P, Smink J, Botnar RM. A new framework for interleaved scanning in cardiovascular MR: application to image-based respiratory motion correction in coronary MR angiography. Magn Reson Med 2015;73:692–696.
20. Greengard L, Lee JY. Accelerating the nonuniform fast Fourier transform. SIAM Rev 2004;46:443–454.
21. Zwart NR, Johnson KO, Pipe JG. Efficient sample density estimation by combining gridding and an optimized kernel. Magn Reson Med 2012;67:701–710.
22. Bracewell RN, Chang K-Y, Jha AK, Wang Y-H. Affine theorem for two-dimensional Fourier transform. Electron Lett 1993;29:304.
23. Etienne A, Botnar RM, Van Muiswinkel AMC, Boesiger P, Manning WJ, Stuber M. "Soap-Bubble" visualization and quantitative analysis of 3D coronary magnetic resonance angiograms. Magn Reson Med 2002;48:658–666.
24. Nehrke K, Bornert P, Manke D, Bock J. Free-breathing cardiac MR imaging: study of implications of respiratory motion-initial results. Radiology 2001;220:810–815.
25. Akçakaya M, Basha TA, Chan RH, Manning WJ, Nezafat R. Accelerated isotropic sub-millimeter whole-heart coronary MRI: compressed sensing versus parallel imaging. Magn Reson Med 2014;71:815–822.
26. Lustig M, Donoho D, Pauly JM. Sparse MRI: The application of compressed sensing for rapid MR imaging. Magn Reson Med 2007;58: 1182–1195.
27. Moghari MH, Roujol S, Henningsson M, Kissinger K V, Annese D, Nezafat R, Manning WJ, Geva T, Powell AJ. Three-dimensional heart locator for whole-heart coronary magnetic resonance angiography. Magn Reson Med 2014;71:2118–2126.
28. Pruessmann KP, Weiger M, Börnert P, Boesiger P. Advances in sensitivity encoding with arbitrary k-space trajectories. Magn Reson Med 2001;46:638–651.
29. Piccini D, Littmann A, Nielles-Vallespin S, Zenge MO. Spiral phyllotaxis: the natural way to construct a 3D radial trajectory in MRI. Magn Reson Med 2011;66:1049–1056.
30. Chan RW, Ramsay EA, Cheung EY, Plewes DB. The influence of radial undersampling schemes on compressed sensing reconstruction in breast MRI. Magn Reson Med 2012;67:363–377.
31. Ingle RR, Wu HH, Addy NO, Cheng JY, Yang PC, Hu BS, Nishimura DG. Nonrigid autofocus motion correction for coronary MR angiography with a 3D cones trajectory. Magn Reson Med 2014;72:347–361.